All-optical switching with bacteriorhodopsin protein coated microcavities and its application to low power computing circuits

Sukhdev Roy,[1,a)] Mohit Prasad,[1,a)] Juraj Topolancik,[2,b)] and Frank Vollmer[2,c)]
[1]*Department of Physics and Computer Science, Dayalbagh Educational Institute, (Deemed University) Dayalbagh, Agra 282 110, India*
[2]*Biofunctional Photonics Group, The Rowland Institute, Harvard University, 100 Edwin H. Land Blvd., Cambridge, Massachusetts 02142, USA*

(Received 15 September 2009; accepted 14 January 2010; published online 12 March 2010)

We show all-optical switching of an input infrared laser beam at 1310 nm by controlling the photoinduced retinal isomerization to tune the resonances in a silica microsphere coated with three bacteriorhodopsin (BR) protein monolayers. The all-optical tunable resonant coupler re-routes the infrared beam between two tapered fibers in 50 μs using a low power (<200 μW) green (532 nm) and blue (405 nm) pump beams. The basic switching configuration has been used to design all-optical computing circuits, namely, half and full adder/subtractor, de-multiplexer, multiplexer, and an arithmetic unit. The design requires 2^n-1 switches to realize n bit computation. The designs combine the exceptional sensitivities of BR and high-Q microcavities and the versatile tree architecture for realizing low power circuits and networks (approximately mW power budget). The combined advantages of high Q-factor, tunability, compactness, and low power control signals, with the flexibility of cascading switches to form circuits, and reversibility and reconfigurability to realize arithmetic and logic functions, makes the designs promising for practical applications. The designs are general and can be implemented (i) in both fiber-optic and integrated optic formats, (ii) with any other coated photosensitive material, or (iii) any externally controlled microresonator switch. [doi:10.1063/1.3310385]

I. INTRODUCTION

The anticipated requirement for ultrahigh speed ultrahigh bandwidth information processing has provided tremendous impetus for realization of all-optical devices and circuits. The advent of nano and bio technologies in the design, synthesis, and characterization of novel materials and structures that include nanophotonics, biophotonics, plasmonics, organic, and silicon photonics, photonic crystals and metamaterials, high-Q microresonators, slow and fast light, and quantum information processing, has opened exciting new possibilities for generation, manipulation, and detection of light along with integration of multiple components and devices to achieve all-optical information processing.[1–7]

Recent years have witnessed a renewed interest in optical computing due to two important advancements, namely, the development of (i) efficient conservative and reversible logic, algorithms, and architectures that exploit the strengths of optics and (ii) novel materials that exhibit high nonlinearities and structures that confine light to low dimensions that facilitates low power nonlinear optics.[8–14] These advancements offer tremendous scope to overcome the impediments to realize optical computing such as cascading components and devices to fabricate circuits and networks in the form of two-dimensional/three-dimensional arrays that are small enough to have low switching energies and high speeds.[15,16]

The flexibility of electronic processing stems from its ability to perform nonlinear operations such as thresholding. In optical processing, nonlinear optical mechanisms play important role in ultrafast optical switches and all-optical logic gates. The integration of photonic components is expected to increase significantly due to emerging novel photonic structures such as microresonators, photonic crystals, and plasmonics.[1–7]

Microcavities have emerged as extremely sensitive and versatile device configurations for a variety of operations due to their high Q-factor, low switching threshold, and ultracompactness.[1,16–20] Optical microcavities confine light to small volumes by resonant circulation. For a coupled, input power P_{in}, the circulating intensity within the resonator is given by $I=P_{in}(\lambda/2\pi n)(Q/V)$ where n is the group index. For a cavity of $Q\sim10^8$ and a mode volume of 500 μm^3 (both obtainable in spheres roughly 40 μm in diameter), the circulating intensity exceeds 1 GW/cm^2 with less than 1 mW of coupled input power.[1]

A very wide range of microresonator shapes have been explored over the years for various applications. The most widely used are rotationally symmetric structures such as Fabry–Perot cavities, spheres, cylinders, disks, torroids, and photonic crystals which have been shown to support very high-Q whispering gallery (WG) modes, whose modal field intensity distribution is concentrated near the dielectric-air interface.[1,16–24]

Devices based on microcavities are already indispens-

[a)]Authors to whom correspondence should be addressed. Tel.: +91-562-2801545. FAX: +91-562-2801226. Electronic addresses: sukhdevroy@dei.ac.in and mohitprasad7@gmail.com.
[b)]Present address: Department of Electrical and Computer Engineering, Northeastern University, 360 Huntington Avenue, Boston, MA 02115. Tel.: +1-617-373-4159. FAX: +1-617-373-8970. Electronic mail: jtopolan@ece.neu.edu.
[c)]Tel.: +1-617 497 4681. FAX: +1-617-497-4627. Electronic mail: vollmer@rowland.harvard.edu.

able for a wide range of applications and studies. By tailoring the microcavity shape, size or material composition, the microcavity can be tuned to support a spectrum of optical modes with required polarization, frequency, and emission patterns.[1,16–24] Some key optical microresonator material systems are Si, SOI, SiO_xN_y, GaAs, InP, GaN, and $LiNbO_3$.[20] Various all-optical logic operations have been shown using Si, GaAs, and InGaAs microcavities.[25,26] The nonlinear optical mechanism implemented in the gates is the change in the refractive index from free charge carriers generated by two photon absorption. Although the change in refractive index in these microcavities is high, the absorption generates heat inside the microcavity due to pump power. The pump and probe power is in milli watts and the Q-factor $\sim 10^4$.[25,26] Recently, a spatially nonblocking optical router with a footprint of 0.07 mm^2 has been demonstrated.[27] The device is dynamically switched using thermo-optically tuned silicon microring resonators with a wavelength shift to power ratio of 0.5 nm/mW. The design can route four optical inputs to four outputs with individual bandwidths of upto 38.5 GHz. These configurations can route a single-wavelength laser and provide a maximum extinction ratio larger than 20 dB.[27]

Silica microcavities have an inherent advantage of high Q-factor, relatively simple fabrication, possible on chip integration and control of the coupling efficiency through taper by the change in the fiber thickness.[1,18–20,23] Fiber optic tapers have been proposed as a means to couple quantum states to or from a resonator onto a fiber.[1] Also the recent demonstration of a fiber-taper-coupled ultrahigh-Q microtoroid on a chip enables integration of wafer based functions with ultralow-loss fiber-coupled quantum devices. The bulk optical loss from silica is also exceptionally low and record Q factors of 8×10^9 (and finesse of 2.3×10^6) have been reported.[1,23] Ultrahigh-Q microtoroidal silica resonators represent a distinct class of optical microresonators with Q's in excess of 10^8.[23] Due to the high Q-factor and the small dimensions, switching at low power is feasible. Moreover, coating the microcavity with a photosensitive material can further lead to switching at ultralow powers.

Recently, all-optical switching in the near infrared with D96N bacteriorhodopsin (BR) mutant coated silica microcavities has been reported, with a Q-factor on BR adsorption $\sim 5\times10^5$.[28] The state of the BR in optical microcavities is controlled by a low power (<200 μW) continuous green pump laser coupled to the microsphere cavity using a tapered fiber.[28,29] The photochromic protein BR found in the purple membrane fragments of *Halobacterium halobium*, has emerged as an outstanding photonic material for practical applications due to its unique multifunctional photoresponse and properties.[28–35] By absorbing green-yellow light, the BR molecule undergoes several structural transformations in a complex photocycle that generates a number of intermediate states.[30–35] The photocycle of D96N-mutant BR is as shown in Fig. 1. After excitation with green-yellow light at 570 nm, the molecules in the initial *all-trans* ground *B*-state get transformed into *J*-state within about 0.5 ps. The species in the *J*-state thermally transforms in 3 ps into the intermediate 13-*cis K*-state, which in turn transforms in about 2 μs into

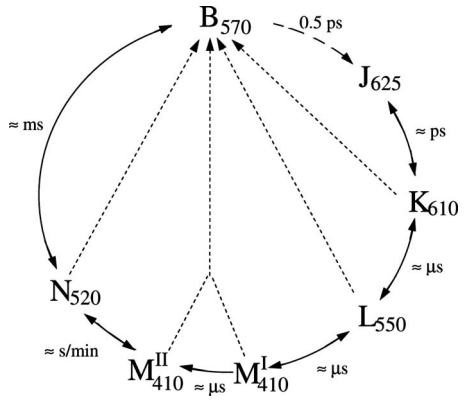

FIG. 1. Schematic of the photochemical cycle of D96N-BR molecule. Subscripts indicate absorption peaks in nanometer. Solid and dashed arrows represent thermal and photoinduced transitions, respectively.

the *L*-state. From the *L*-state, BR thermally relaxes to the M^{I}-state within 8 μs and undergoes irreversible transition to the M^{II}-state. The molecules then relax to the *N* state in a few seconds or minutes and finally to the initial *B*-state within about 10 ms. An important feature of all the intermediate states is their ability to be photochemically switched back to the initial *B*-state by shining light at a wavelength that corresponds to the absorption peak of the intermediate in question.[30–35] The wavelength in nm of the absorption peak of each species is shown as a subscript in Fig. 1. The D96N-BR photocycle exhibits a much longer time (s/min) compared to wild-type BR ($\sim$ms). Photoinduced molecular transitions in BR can be used to reversibly configure an ultrasensitive micron scale photonic component in which the optical response is resonantly enhanced.

Cascading to integrate a large number of all-optical components such as switches, logic gates etc., is a complex problem and a major obstacle in the development of a complete all-optical computing system.[8,14] Branching of signals all-optically among various logic devices is a critical task. Theoretical schemes suggesting alternative solutions for parallel generation of logic gates have been recently reported in literature.[36–39] An effective method for cascading involves the tree architecture. It is a multiplying system of a single straight path into several distributed branches and sub-branch paths. Shen and Wu have demonstrated that reconfigurability can be introduced into designs of all-optical logic circuits by electro-optic switches.[40] Recently, Kodi and Louri have demonstrated that optical based system architecture shows better performance than electrical interconnects for uniform and nonuniform patterns without the application of reconfiguration techniques.[41] Even with the application of reconfiguration techniques, the dynamically reconfigurable optoelectronics provides much better performance for all communication patterns. Caulfield *et al.*[42] have also proposed an electro-optical logic system with silicon-on-insulator (SOI) resonant structures. Thus, low power BR-coated microcavity switch in a suitable architecture can also be useful to achieve all-optical computing.

The key objective of this paper is to (i) demonstrate faster all-optical switching in BR-coated microcavities and (ii) to combine the advantages of BR-coated microcavity

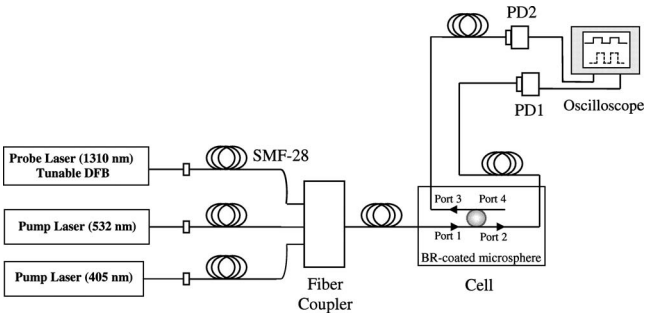

FIG. 2. Experimental setup of all-optical switching in BR-coated microcavity switch.

switches with tree architecture and propose general designs for optically controlled microcavity based computing circuits, i.e., all-optical arithmetic and combinatorial circuits that can be reconfigured to realize different logic and arithmetic operations in parallel. We show fast switching in BR-coated microcavity switch by injecting an additional blue laser beam (405 nm) in synchronization with green laser beam (532 nm). The whole logic unit consists of identical switches and the horizontal and vertical extension of the designs can also be easily realized by suitable selection of branches and sub-branches.

II. EXPERIMENTAL SETUP OF BR-COATED MICROCAVITY SWITCH

The schematic diagram of the experimental setup for all-optical switching with BR-coated microcavity is shown in the Fig. 2. A 300 μm silica microsphere ($Q \sim 2 \times 10^6$) was formed by melting the tip of a single mode fiber in a butane nitrous oxide flame. Three monolayers of BR mutant D96N (Munich Innovative Biomaterials, Munich, Germany) were adsorbed onto the microsphere surface using alternate electrostatic deposition of cationic poly(dimethyldaiallyl) ammoniumchloride (PDAC) and anionic BR membranes. In each cycle a single oriented PDAC/BR monolayer ($\sim$55 Å thick) was self-assembled onto the microcavity surface.[28] The BR adsorption process slightly degraded the microcavity Q to $\sim 5 \times 10^5$, which was caused by the introduction of the scattering impurities during each drying process. Two parallel, single mode fibers held at 250 μm apart in a standard 1 cm acid resistant polystyrene cuvette were tapered by hydrofluoric acid erosion. Once etched, the fibers were immersed in 0.01 M phosphate buffered saline with pH=7.4. The BR-coated microsphere was then spring loaded between the two tapered fibers. Resonant modes were excited with a distributed feedback laser, operating around 1310 nm, connected to port 1 via single mode fiber (SMF-28, Dow-Corning, Midland MI) through fiber coupler. Green pump beam at wavelength 532 nm and a blue pump beam at wavelength 405 nm were injected into port 1 of the switch. To determine the resonant wavelength, the modulation current was periodically scanned at 100 Hz with a sawtooth shaped function. Photodiodes PD1 and PD2 connected to fiber ports 2 and 3 were used to monitor the transmitted intensity of the probe and a spectrum containing 1000 points was recorded every $\sim$200 ms with a LABVIEW program.

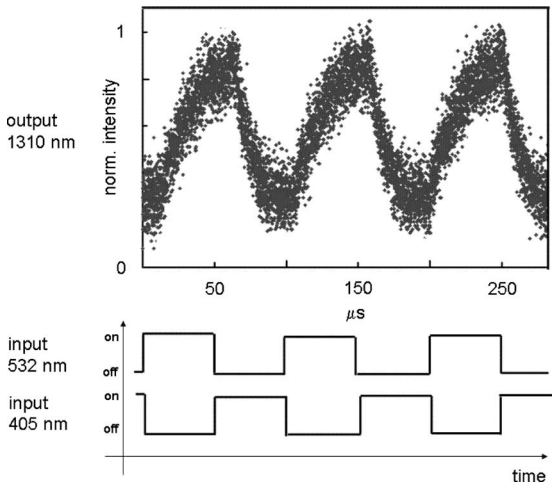

FIG. 3. Variation in the signal probe beam (operating at 1310 nm) with the modulating pump laser beams at 532 nm and 405 nm.

III. RESULTS AND DISCUSSION

A. All-optical switching in BR-coated microcavity

In the BR-coated microcavity switch, the switching of input signal operating at wavelength 1310 nm between the output ports (2 and 3) is photo-induced with a fiber-coupled green pump laser (at 532 nm) which controls the conformational state of the adsorbed BR. The molecularly functionalized microcavity thus redirects the flow of near-infrared light beam between two optical fibers. With the pump OFF, the probing light from input port 1 is detuned from resonance and is directly transmitted into the output port 2. The pump evanescently excites WG modes (WGM) propagating around the microsphere's equator, inducing photoisomerization along their path. A low green continuous wave (cw) laser ($<$200 μW at 532 nm) is sufficient for this purpose as its effective absorption is resonantly enhanced. Isomerization reduces the retinal polarizability, tuning the peak/trough of the resonance to match the wavelength of the infrared probe which is then rerouted into the output port 3.[28,29]

The transmitted spectra exhibited an extinction of -9.4 dB in port 2 and a 9.8 dB increase in transmission in port 3. In order to achieve fast switching, a blue light beam of same intensity was injected into the BR-coated microcavity switch in synchronization with a green pump laser beam. The blue light beam (405 nm) helps in truncating the photocycle of the BR molecules at the M intermediate state, which is near to its peak absorption wavelength of 410 nm, which results in a faster switch-off. Fig. 3 shows the variation in the signal probe beam operating at 1310 nm in BR-coated microcavity with the modulating green and blue pump signals operating at wavelengths 532 and 405 nm respectively. The present configuration results in faster all-optical switching (ON/OFF) $\sim \mu$s as compared to our previous experimental results where switch ON/OFF was shown to be $\sim \mu$s/s.[28] The switching dynamics is governed by the speed of the BR photochromic transitions. The fastest switching time with alternating pump sources (532 and 405 nm) was limited to 50 μs since the transition time for D96N-BR mutant was 50 μs ($B \rightarrow M$) and 200 ns ($M \rightarrow B$). D96N-BR is known to

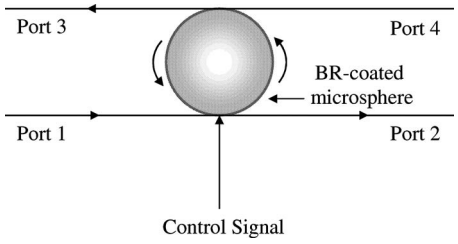

FIG. 4. Schematic of BR-coated microcavity switch as a four-port resonant coupler.

exhibit a much longer M-state lifetime as compared to wild-type BR.[30–35] The switching time can further be reduced by tailoring the BR intermediate lifetimes and/or phototransitions or exploiting ultrafast photochromic transitions in other organic molecules such as diarylethenes. The ultrahigh sensitivity of both microresonators and BR protein configuration results in switching at very low powers. The 200 μW switching power is an upper limit that can be further reduced by working with resonantly coupled coherent pump sources. This, however, would add another level of complexity to the control architecture. Another level of complexity or control can be added by working with the polarization states of BR.[29] Hence, the silica microcavity in contact between two tapered fibers serves as a four-port tunable resonant coupler as shown in Fig. 4. Here, port 1 serves for input as well as for control signal, while ports 2 and 3 act as output ports. The various possible states have been listed in Table I.

IV. DESIGN OF ALL-OPTICAL COMPUTING CIRCUITS

The all-optical BR-coated microcavity switch with a single control signal at 532 nm or in conjunction with a 405 nm can be used as a building block for designing higher computing circuits such as half and full adder-subtractor, (de)-multiplexer (de-MUX), multiplexer (MUX) and arithmetic unit (AU).

A. Half-adder/subtractor

A half-adder/subtractor is a circuit that adds and subtracts two bit binary numbers. Fig. 5 shows the architecture of a half-adder/subtractor based on BR-coated microcavity switches S1, S2, and S3. Here X and Y act as optical control signals operating at wavelength 532 nm with a power of 200 μW. A laser source (LS) is coupled at port (1) of switch S1. The cw light from the LS acts as an input signal to the switch S1. When the LS is switched-OFF there is no light detected in any of the output ports of the architecture.

TABLE I. Truth table of Fig. 4.

Input signal (1310 nm)	Control signal (532 nm)	Port 3	Port 2
0	0	0	0
0	1	0	0
1	0	0	1
1	1	1	0

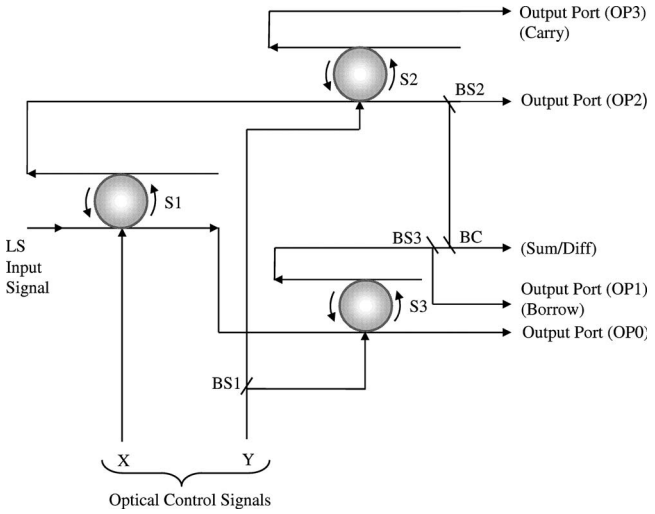

FIG. 5. Schematic of an all-optical logic generator circuit that also performs half-adder/subtractor operations (BS=Beam splitter, BC=Beam combiner, and LS=Laser source).

When the LS is switched ON and both the optical control signals are zero, i.e., X=0 and Y=0, no light is incident on the BR-microcavity switches. As BR is in its ground state hence, the input signal by-passes switches S1 and S3 and emerges at output port OP0. The logic generated at OP0 =X′Y′, as shown in Table II.

Now, when X=0 and Y=1, light is incident on BR-coated microcavity switches S2 and S3 and triggers the conformational changes in BR. The control signal Y activates S2 and S3. The input signal passes from switch S1 to the input of S3 and gets redirected to output port OP1. The logic generated at OP1=X′Y, as shown in Table II. Considering the values taken by optical control signals as X=1, Y=0, now, the input signal gets switched at S1 and emerges at OP2 that corresponds to logic XY′. Similarly, when optical control signals X=1, and Y=1, i.e., all the three switches are activated, the input signal emerges from OP3 via switches S1 and S2. The logic generated at OP3=XY, as shown in Table II.

Different logic operations can be realized by combining output of these ports. For instance, a combination of signals OP0 with OP1 results in X′ logic operation as (X′Y′) +(X′Y)=X′ (Y′+Y)=X′ since (Y′+Y)=1. Combination of different outputs also result in X, Y, X′, Y′, XOR′, XOR, X+Y′, X′+Y, X′+Y′, X+Y, X′Y, XY, X′Y′, XY′, T, and F logic operations.

This architecture in combination with beam splitters and combiners can also result in an all-optical half-adder and subtractor circuit as shown in Fig. 5. Considering Table II, if we combine light signals from OP1 and OP2 through a beam combiner, it results into an XOR operation, which is the "sum" bit of half-adder. The "carry" bit can be obtained from OP3. In the case of half-subtractor, the "difference" bit is obtained by combining OP1 and OP2, whereas the "borrow" bit can be obtained from output port OP1.

B. Full-adder/subtractor

An all-optical full-adder/subtractor is capable of adding and subtracting three-input bits. To design an all-optical full-

TABLE II. Logic generation at different output ports.

Optical control signals		Output at different ports				Sum/diff
X	Y	OP0 (X′Y′)	OP1 (X′Y) (Borrow)	OP2 (XY′)	OP3 (XY) (Carry)	OP1+OP2 (X′Y+XY′)
0	0	1	0	0	0	0
0	1	0	1	0	0	1
1	0	0	0	1	0	1
1	1	0	0	0	1	0

adder/subtractor circuit, we cascade four additional switches S4 to S7 and use an additional control signal Z as shown in Fig. 6. Now, we have eight different input combinations of X, Y, and Z for implementation. Depending on the state of input variables f (X, Y, Z), the output is obtained from one of the output ports OP0 to OP7. The truth table of full-adder and subtractor for three-input binary variables is given in Table III. In the case of the full addition, we have two outputs, the sum and the carry. Here, sum is obtained from Σf (1, 2, 4, 7) and carry from Σf (3, 5, 6, 7). In the case of full subtraction, we have two outputs, the difference and the borrow. We obtain the difference from Σf (1, 2, 4, 7) and borrow from Σf (1, 2, 3, 7).

By combining the output of ports OP1, OP2, OP4, and OP7, we can obtain the sum, whereas combination of output ports OP3, OP5, OP6, and OP7 gives the carry for full adder. Similarly, the combination of output ports OP1, OP2, OP4, and OP7 gives the difference whereas the combination of output ports OP1, OP2, OP3, and OP7 gives the borrow for full subtractor. Thus, this architecture works as an all-optical full adder and subtractor.

C. DE-MUX and MUX

A DE-MUX is a circuit which is used to de-multiplex an input signal from one input channel to one of the many output channels via select lines. The select lines decide the routing of the input signal to the desired output channel. Interestingly, the circuit shown in Fig. 5 can also function as a DE-MUX without the need of beam splitters BS2 and BS3. Figs. 7(a) and 7(b) show the block diagram and design of a DE-MUX. As discussed earlier, a combination of the control signals/select lines decides the output port from which the emerging signal emerges, conforming to a 1: 4 DE-MUX with the truth table as shown in Table IV.

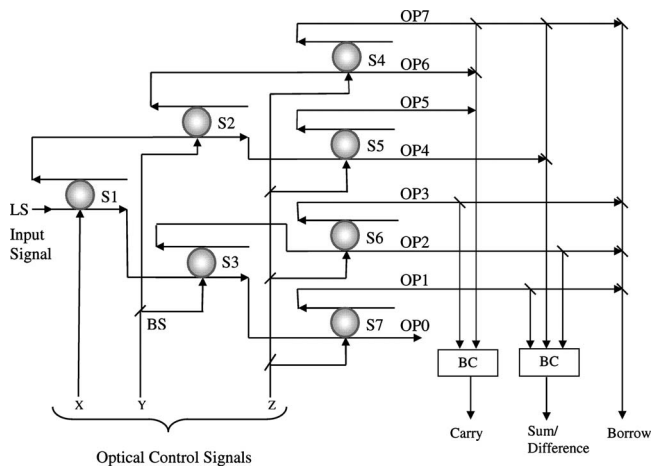

FIG. 6. Design of an integrated all-optical full-adder and subtractor circuit (BS=Beam splitter, BC=Beam combiner, OP=Output port, and LS=Laser source).

On the other hand, a multiplexer (MUX) is a fundamental combinatorial and function generator circuit which is used to multiplex input signals from a number of input channels to a single output channel depending on the value of the select lines. The block diagram of a 4:1 MUX is shown in Fig. 8(a). The same DE-MUX configuration can also be used to realize a 4:1 MUX which is explicitly shown in Fig. 7(b)) with dashed lines. In this case, the inputs IP0 to IP3 are incident on switches S2 and S3 from the right and the output is at output port OP on the left. Based on the combination of select lines X and Y, one of the inputs gets switched and passes through output port OP. For case X=0, Y=0, OP0 reaches OP. When X=0, Y=1, IP1 reaches OP. For case X=1, Y=0, IP2 reaches OP. Finally, for X=1, Y=1, IP3 reaches OP.

Since all inputs are considered at the same wavelength of 1310 nm, in order to distinguish the four inputs they can either be at different powers or they can have different bit rates and the select lines can be modulated at different frequencies to tune the resonant couplers at corresponding frequencies for selection. In this case, X=Y=0 selects input from IP0, X=0, Y=1 (at frequency υ_1 corresponding to frequency of input at IP1) selects IP1, and for X=1, Y=0 (at frequency υ_2 corresponding to frequency of input at IP2) selects IP2. For X=Y=1, we consider X=Y (at frequency υ_3 corresponding to input at IP3), which selects IP3 at OP. In this case IP0 would also reach OP and would have to be filtered to obtain the input signal at IP3.

Another design of a MUX is shown in Fig. 8(b). For implementation of this 4:1 MUX, we cascade four more BR-coated microcavity switches S4 to S7, with X and Y as the two select lines and IP0 to IP3 as the four data inputs.

Case 1: X=0, Y=0. The input signal moves from port 1 of switch S1 to S7 and gets switched at S7 to emerge at OP if IP0 is in state 1, else it passes by to port 2 of S7. Thus, data input IP0 can be sent to OP by setting X=Y=0.

Case 2: X=0, Y=1. The input signal propagates from port 1 of switch S1 to S3, from where it is re-routed to S6. Now, at S6, it gets switched to emerge at OP or not, depending on the state of IP1.

Case 3: X=1, Y=0. In this case, the input signal

TABLE III. Truth table for realization of full-adder/subtractor.

Optical control signals			Output at different ports								Sum/diff	Carry	Borrow
X	Y	Z	OP0	OP1	OP2	OP3	OP4	OP5	OP6	OP7	ΣOP(1,2,4,7)	ΣOP(3,5,6,7)	ΣOP(1,2,3,7)
0	0	0	1	0	0	0	0	0	0	0	0	0	0
0	0	1	0	1	0	0	0	0	0	0	1	0	1
0	1	0	0	0	1	0	0	0	0	0	1	0	1
0	1	1	0	0	0	1	0	0	0	0	0	1	1
1	0	0	0	0	0	0	1	0	0	0	1	0	0
1	0	1	0	0	0	0	0	1	0	0	0	1	0
1	1	0	0	0	0	0	0	0	1	0	0	1	0
1	1	1	0	0	0	0	0	0	0	1	1	1	1

switches at S1 and reaches S5 which is controlled by IP2 and hence reaches OP if IP2=1.

Case 4: X=1, Y=1. In this case, the input signal again switches at S1 and reaches OP if S4 is activated by IP3. The corresponding truth table for 4:1 MUX is shown in Table V.

D. AU

AU is a versatile integrated circuit which can perform different arithmetic functions. An all-optical AU can also be designed by integrating a combination of BR-coated microcavity switches, full-adders, and MUXs discussed earlier. The number of functions performed by the AU depends on the number of select inputs. The optical circuit shown in Fig. 9 can perform eight different arithmetic functions with two four bit numbers X ($X_3X_2X_1X_0$) and Y ($Y_3Y_2Y_1Y_0$). It gives the output Z ($Z_3Z_2Z_1Z_0$) depending on the value of three select inputs (S_1, S_0, and C_{in1}) which operate at 532 nm. This scheme can be extended for n bit numbers. We consider X ($X_3X_2X_1X_0$) and Y ($Y_3Y_2Y_1Y_0$) operating at 532 and 1310 nm, respectively. The input Y ($Y_3Y_2Y_1Y_0$) is fed after wavelength conversion to the full adders FA1 to FA4. Considering an example, with X=1011 ($X_3X_2X_1X_0$) and Y=1001 ($Y_3Y_2Y_1Y_0$), eight different operations with four subsidiary functions can be realized that are shown in Table VI.

Case 1(a): S_1=0, S_0=0, and C_{in1}=0. As the select lines are not activated, the input line IP0 of all the MUXs will be selected. IP0 of all the MUXs are connected to Y and hence OP0-OP3 will have values Y_0-Y_3, respectively. These outputs after wavelength conversion to 532 nm act as inputs of the full adders, FA1-FA4, respectively. All the full-adders receive the other input X directly. In this case X_0 is directly

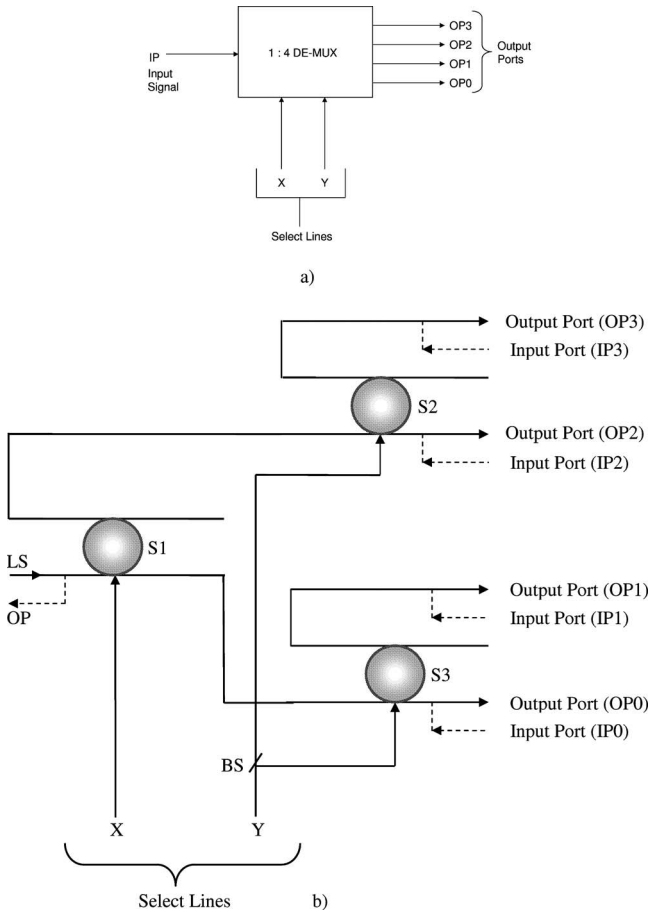

FIG. 7. Design of all-optical DE-MUX (LS=laser source, BS=Beam splitter) (a) block diagram and (b) schematic. Dashed lines signify MUX operation.

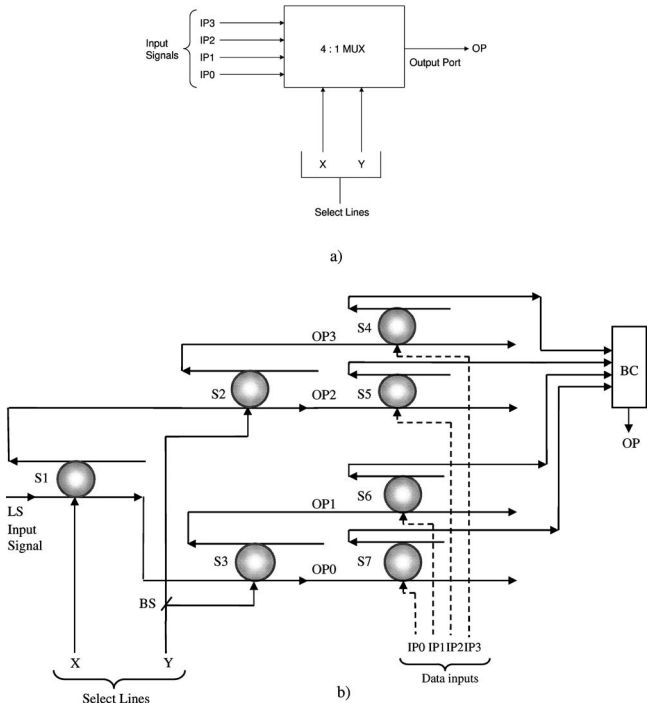

FIG. 8. Design of all-optical MUX (BS=Beam splitter, LS=Laser source) (a) block diagram and (b) schematic.

TABLE IV. Truth table of 1: 4 DE-MUX.

Input signal	Select lines/control signals		Data outputs			
LS	X	Y	OP0	OP1	OP2	OP3
0	0	0	0	X	X	X
1	0	0	1	X	X	X
0	0	1	X	0	X	X
1	0	1	X	1	X	X
0	1	0	X	X	0	X
1	1	0	X	X	1	X
0	1	1	X	X	X	0
1	1	1	X	X	X	1

connected to one input (i.e., X) of the FA1 and $C_{in1}=0$. Now, for the example considered, as the $X_0=1$, $Y_0=1$ and $C_{in1}=0$, $Z_0=0$ and $C_{out1}=1$. In FA2, $C_{in2}=1$ and X and Y are 1 and 0, respectively (as $X_1=1$, $Y_1=0$). In this case, $Z_1=0$ and $C_{out2}=1$. Similarly, in FA3, as $C_{in3}=1$, and $X=Y=0$ (as $X_2=0$ and $Y_2=0$), $Z_2=1$ and $C_{out3}=0$. Finally, in FA4, $C_{in4}=0$, and $X=Y=1$ (as $X_3=1$ and $Y_3=1$) that yields $Z_3=0$ and $C_{out4}=Z_4=1$. The final output (Z) is 10100 ($Z_4Z_3Z_2Z_1Z_0$) which verifies the binary addition (X+Y) of two four bit numbers.

Case 1(b): $S_1=0$, $S_0=0$, and $C_{in1}=0$. As one of the input X=0000, the output is merely Y.

Case 2(a): $S_1=0$, $S_0=0$, and $C_{in1}=1$. All the operations are similar to that of case 1(a), with the difference that the carry in C_{in1} of the FA is 1. Since, $X_0=1$, $Y_0=1$ the output of FA1, i.e., $Z_0=1$ and $C_{out1}=1$. Other FAs' perform in a similar manner and the final output is 10101 ($Z_4Z_3Z_2Z_1Z_0$). Hence, the AU performs the operation of addition with carry.

Case 2(b): $S_1=0$, $S_0=0$, and $C_{in1}=1$. As one of the input X=0000, the function generated by the AU is Y+1.

Case 3(a): $S_1=0$, $S_0=1$, and $C_{in1}=0$. As the select inputs $S_1=0$, $S_0=1$, the input data line IP1 of each MUX will be selected. As the select input $Y_0=1$, the signal at IP1 will be complement of Y_0 (i.e., Y_0') due to switching at S6. Similarly, Y_1, Y_2, and Y_3 act as control inputs of the switches S8, S10, and S12 and the corresponding input port IP1 of all the MUXs receives the complement values of Y_0-Y_3, respectively. These are then wavelength converted to 532 nm to form inputs Y of FA1-FA4, respectively. Now in FA1, carry in $C_{in1}=0$ and the inputs X=1 (as $X_0=1$), and Y=0, which is the complement of Y_0 (as $Y_0=1$). Hence, $Z_0=1$ and $C_{out1}=0$. In FA2, $C_{in2}=0$ and $X=Y=1$ (as $X_1=1$ and $Y_1=0$) hence $Z_1=0$ and $C_{out2}=1$. Similarly, in FA3, $C_{in3}=1$ and the input X=0 (as $X_2=0$), and the input Y=1 (as $Y_2=0$), leads to $Z_2=0$, and $C_{out3}=1$. Finally in FA4, $C_{in4}=1$, X=1, and Y=0 results in $Z_3=0$ and $C_{out4}=Z_4=1$. Hence, the final output Z is 10001 ($Z_4Z_3Z_2Z_1Z_0$) which confirms to the third operation (X+Y′) as given in Table VI.

Case 3(b): $S_1=0$, $S_0=1$, and $C_{in1}=0$. As one of the input X=0000, the function generated at the output is Y′.

Case 4(a): $S_1=0$, $S_0=1$, and $C_{in1}=1$. All the operations are similar to that of case 3(a), with a difference that the carry in of FA1 is 1 as the select input $C_{in1}=1$. Now, the input $X=X_0=1$ and the input $Y=Y_0'=1$, results in $Z_0=0$, and $C_{out1}=1$. Hence, output Z=10010. In this case the AU uses 2's complement method of subtraction. As the final carry (C_{out4}) from FA4 is one (i.e., $Z_4=1$), the result is positive and the final carry is to be discarded. Hence, the final result is positive as its value is 0010 ($Z_3Z_2Z_1Z_0$), which also verifies the 2's complement subtraction operation (X+Y′+1) as given in Table VI. Now, if we consider X=1001 ($X_3X_2X_1X_0$) and Y=1011 ($Y_3Y_2Y_1Y_0$), then the AU generates the output Z as 01110 ($Z_4Z_3Z_2Z_1Z_0$). As the final carry is 0 (i.e., $Z_4=0$), the result is negative and the final carry Z_4 is to be discarded.

Case 4(b): $S_1=0$, $S_0=1$, and $C_{in1}=0$. In this case, as X=0000, the function generated at the output is Y′+1.

Case 5: $S_1=1$, $S_0=0$, and $C_{in1}=0$. As the select inputs $S_1=1$ and $S_0=0$, the input data line IP2 will be selected for all the MUXs. Port 2 of switch S1 will receive light, which logically is the complement of control signal C_{in1} (i.e., C_{in1}').

TABLE V. Truth table for 4: 1 MUX.

Data inputs				Select lines/control signals		Outgoing signal	
IP0	IP1	IP2	IP3	X	Y	O/S	Selected data input
0	X	X	X	0	0	0	**IP0**
1	X	X	X	0	0	1	
X	0	X	X	0	1	0	**IP1**
X	1	X	X	0	1	1	
X	X	0	X	1	0	0	**IP2**
X	X	1	X	1	0	1	
X	X	X	0	1	1	0	**IP3**
X	X	X	1	1	1	1	

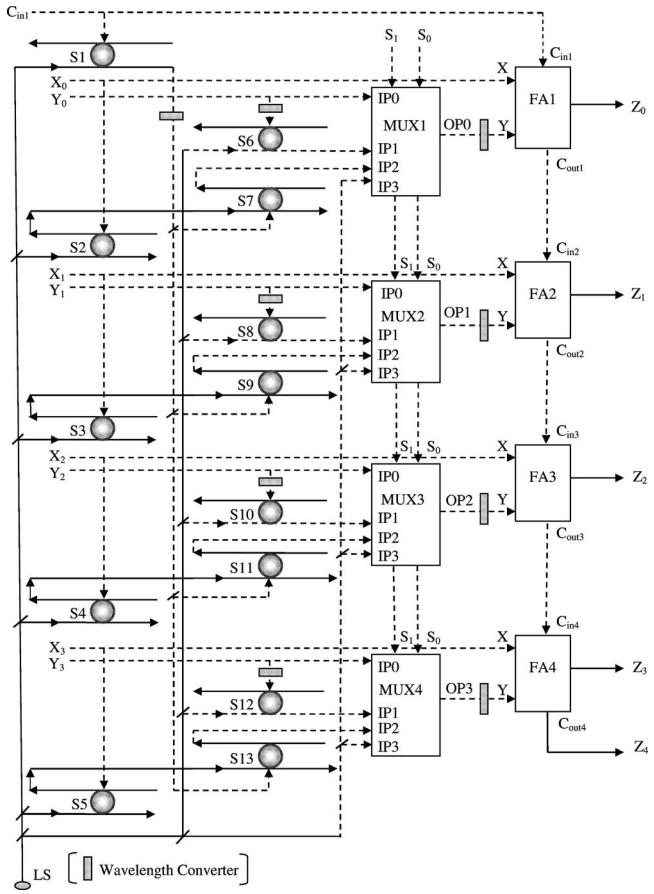

FIG. 9. Design of all-optical AU (MUX=Multiplexer, and FA=Full-adder).

Again X_0-X_3 act as control inputs for switches S2-S5, respectively. Port 2 of switch S1 (i.e., C'_{in1}) is connected to switches S7, S9, S11, and S13 through wavelength converters. The input port IP2 of MUX1-MUX4 will receive the values which will be equal to XC'_{in1} and generate the values as X_0-X_3, respectively (since $XC'_{in1}=X$ as $C_{in1}=0$). Now, in FA1, $C_{in1}=0$, and the other two inputs $X=Y=1$ (as $X_0=1$ is independent of Y_0) hence $Z_0=0$, and $C_{out1}=1$. In FA2, $C_{in2}=1$ and $X=Y=1$ (as $X_1=1$) that yields $Z_1=1$ and $C_{out2}=1$. Similarly, $Z_2=1$, $Z_3=0$, and $Z_4=1$. The final output Z is 10110 ($Z_4Z_3Z_2Z_1Z_0$), which verifies the double operation (2X) of a four bit number (X) as given in Table VI.

Case 6: When $S_1=1$, $S_0=0$, and $C_{in1}=1$. In this case also, select inputs select the input data line IP2 for all the MUXs. As the select input $C_{in1}=1$, the input data line IP2 of all the MUXs receives the value 0 ($XC'_{in1}=0$ since select input $C_{in1}=1$). Hence, the input $Y=0$ for all the full-adders. In FA1, $C_{in1}=1$, and $X=1$, $Y=0$ (as $X_0=1$ and $X_0C'_{in}=0$), which results in $Z_0=0$ and $C_{out1}=1$. In FA2, $C_{in2}=1$, and $X=1$, $Y=0$ (as $X_1=1$ and $X_1C'_{in2}=0$), to yield $Z_1=0$ and $C_{out2}=1$. Similarly in FA3, $C_{in3}=1$, and $X=0$, $Y=0$ (as $X_2=0$ and $X_2C'_{in3}=0$) hence $Z_2=1$ and $C_{out3}=0$. Finally, in FA4, $C_{in4}=0$, and $X=1$, $Y=0$ yields $Z_3=1$ and $C_{out4}=Z_4=0$. The final output Z is 01100 ($Z_4Z_3Z_2Z_1Z_0$), which verifies the increment operation (X+1) of a four bit number (X) as given in Table VI.

Case 7: $S_1=1$, $S_0=1$, and $C_{in1}=0$. As the select inputs $S_1=1$, $S_0=1$, now the input data line IP3 is selected for MUX1-MUX4. Here, the IP3 line of all the MUXs is connected to the input signal which is always in the high state. So, all the MUXs generate the output as 1. Thus, input $Y=1$ for all the full-adders. Now, in FA1, $C_{in1}=0$ and input $X=1$ ($X_0=1$) and input $Y=1$ (as MUX1 generates output 1) hence $Z_0=0$ and $C_{out1}=1$. In FA2, $C_{in2}=1$ and inputs $X=Y=1$, resulting in $Z_1=1$ and $C_{out2}=1$. Similarly, in FA3, $C_{in3}=1$, and $X=0$ (as $X_2=0$) and $Y=1$, which yields $Z_2=0$ and $C_{out3}=1$. Finally in FA4, $C_{in4}=1$, $X=1$ (as $X_3=1$) and $Y=1$ to give $Z_3=1$ and $C_{out4}=Z_4=1$. The circuit generates the output Z as 11010 ($Z_4Z_3Z_2Z_1Z_0$) which is the decrement operation (X-1) of a four bit number X as given in Table VI.

Case 8: $S_1=1$, $S_0=1$, and $C_{in1}=1$. Now all the select inputs are 1 hence all the operations are similar to that of Case 7 with the difference that $C_{in1}=1$. In FA1, as input $X=1$ (as $X_0=1$) and input $Y=1$, it generates $Z_0=1$ and $C_{out1}=1$. In FA2, as $C_{in2}=1$ and $X=Y=1$, $Z_1=1$ and $C_{out2}=1$. Similarly, FA3 and FA4 yields $Z_2=0$ and $Z_3=1$, respectively, hence $Z_4=C_{out4}=1$. The circuit gives the output Z as 11011 ($Z_4Z_3Z_2Z_1Z_0$) and the final carry is to be discarded as Z is a four bit number, to give the final result as 1011 ($Z_3Z_2Z_1Z_0$), which verifies the transfer operation of a four bit number as given in Table VI.

The AU thus performs eight primary and four subsidiary functions. Since, nearly all the input power is switched by photoinducing the BR-coated microcavities, multiple switches can be cascaded to result in a large fanout. The microcavities can be tuned to operate at 1064 nm such that the second harmonic generation at the wavelength converters can result in efficient conversion of light at 532 nm. Operating the control signals at 570 nm, which is the peak absorp-

TABLE VI. Arithmetic functions realized using all-optical AU.

S.No.	Functions generated	Select inputs S_1	S_0	C_{in1}	Selected input	Inputs: X, Y output: Z ($Z_4Z_3Z_2Z_1Z_0$)
1	Binary-addition	0	0	0	IP0	Z=X+Y, Z=Y; if X=0
2	Addition with carry	0	0	1		Z=X+Y+1, Z=Y+1; if X=0
3	Subtraction with borrow	0	1	0	IP1	Z=X+Y′, Z=Y′; if X=0
4	Subtraction (2's complement)	0	1	1		Z=X+Y′+1, Z=Y′+1; if X=0
5	Double of X	1	0	0	IP2	Z=2 X
6	Increment of X	1	0	1		Z=X+1
7	Decrement of X	1	1	0	IP3	Z=X−1
8	Transfer of X	1	1	1		Z=X

tion wavelength of BR, would also lead to lower switching powers. The proposed designs of the MUX and DE-MUX are reversible, in the sense that the circuit can be used from the input or from the output side.

The switching of the infrared wavelength (1310 nm) probe with the controlled pump operating at 532 nm with or without 405 nm may find potential applications in telecommunications as well. The microresonator cavity can be tailored to effectively switch a desired wavelength. Cascading can easily be achieved as BR-coated microcavity switches dissipate less power. With the powerful capabilities of nanobiotechnological techniques, the BR response can be tailored to meet device specifications.[33]

Coating the microcavities with a photosensitive material is of critical value, as the material should exhibit high sensitivity, high absorption, fast dynamics, high photo, and thermal stability and potential to tailor its properties. BR protein is a natural photochromic material that exhibits this unique combination of properties for practical realization. Although proposed designs can be realized with dual-ring switches and other interferometric configurations, single BR based microcavity switch has advantages in terms of simple geometry, ease of fabrication, high thermal and photostability, high fan out, cost-effectiveness, and low power operation.

V. CONCLUSION

In this paper, we have shown all-optical switching in a BR-coated microcavity switch with two pump beams at 532 and 405 nm, to achieve faster switching. We have also presented a theoretical scheme which combines the advantages of BR, the high-Q microcavities and the tree architecture for designing low power all-optical, half and full-adder/subtractor, DE-MUX, MUX and AU. These schemes are general and can be implemented (i) in both fiber optic and integrated optic formats, (ii) with any other coated photosensitive material, or (iii) any externally controlled microresonator switch. These schemes can easily be extended and implemented for any higher number of input digits, by proper interconnection of BR-coated microcavity switches, using vertical and horizontal extension of the tree and by suitable branch selection. The combined advantages of high Q-factor, tunability and compactness of microresonators and the high sensitivity, absorption, and stability of BR makes low power switching possible. In addition to this, the flexibility of cascading switches in tree architectures to form circuits and reversibility and reconfigurability to realize arithmetic and logic operations, makes the designs promising for practical applications. The proposed designs can yield large computing circuits and networks within milliwatt power budget. To realize n bit computation the proposed design requires only 2^n-1 switches.

The change in the refractive index in a BR-coated microcavity switch depends on the wavelength of the control beam, making the switches tunable. The proposed designs propose a new paradigm for all-optical computing based on hybrid nanobiophotonic integrated devices employing biomolecules to perform photonic functions.

[1] K. J. Vahala, Nature (London) **424**, 839 (2003).
[2] J. L. O'Brien, Science **318**, 1567 (2007).
[3] T. Baba, Nat. Photonics **2**, 465 (2008).
[4] A. M. C. Dawes, D. J. Gauthier, S. Schumacher, N. H. Kwong, R. Binder, and A.L. Smirl, Laser Photonics Rev. **4**, 221 (2010)
[5] K. Szacilowski, Chem. Rev. **108**, 3481 (2008).
[6] L. Tsybeskov, D. J. Lockwood, and M. Ichikawa, Proc. IEEE **97**, 1161 (2009).
[7] Z. Zhou, Electron. Lett. (Spl. Suppl.-Adv. Si Photonics) June, 2 (2009).
[8] H. Abdeldayem and D. O. Frazier, Commun. ACM **50**, 60 (2007).
[9] *Optical Super Computing*, Lecture Notes in Computer Science Vol. 5172, edited by H. J. Caulfield, S. Dolev, T. Haist, and M. Oltean, (Springer, Berlin, 2008) p. 1.
[10] H. J. Caulfield, S. Dolev, and W. M. J. Green, Appl. Opt. **48**, 1 (2009).
[11] H. J. Caulfield, L. Qian, C. S. Vikram, A. Zavalin, K. Chouffani, J. Hardy, W. J. Mccurdy, and J. Westphal, Adv. Imaging Electron Phys. **142**, 1 (2006).
[12] J. Hardy and J. Shamir, Opt. Express **15**, 150 (2007).
[13] H. John Caulfield, R. A. Soref, L. Qian, A. Zavalin, and J. Hardy, Opt. Commun. **271**, 365 (2007).
[14] R. Lytel, H. L. Davidson, N. Nettleton, and T. Sze, Proc. IEEE **88**, 758 (2000).
[15] D. Woods and T. J. Naughton, Appl. Math. Comput. **215**, 1417 (2009)
[16] X. Hu, P. Jiang, C. Ding, H. Yang, and Q. Gong, Nat. Photonics **2**, 185 (2008).
[17] M. Notomi, E. Kuramochi, and T. Tanabe, Nat. Photonics **2**, 741 (2008).
[18] F. Vollmer and S. Arnold, Nat. Methods **5**, 591 (2008).
[19] A. Chiasera, Y. Dumeige, P. Feron, M. Ferrari, Y. Jestin, G. N. Conti, S. Pelli, S. Soria, and G. C. Righini, "Spherical whispering-gallery-mode microresonators", Laser Photonics Rev. (in press).
[20] T. M. Benson, S. V. Boriskina, P. Sewell, A. Vukovic, S. C. Greedy, and A. I. Nosich, in *Frontiers in Planar Lightwave Circuit Technology: Design Simulation and Fabrication*, Vol. 216, edited by S. Janz, J. Ctyroky, and S. Tanev (Springer, Dodrecht, The Netherlands, 2006) p. 39.
[21] V. S. Ilchenko and A. B. Matsko, IEEE J. Sel. Top. Quantum Electron. **12**, 15 (2006).
[22] A. B. Matsko, A. A. Savchenkov, D. Strekalov, V. S. Ilchenko, and L. Maleki, IPN Progress Report No. 42–162, 1 (2005).
[23] D. K. Armani, T. J. Kippenberg, S. M. Spillane, and K. J. Vahala, Nature (London) **421**, 925 (2003).
[24] S. Manipatruni, C. B. Poitras, Q. Xu, and M. Lipson, Opt. Lett. **33**, 1644 (2008).
[25] Q. Xu and M. Lipson, Opt. Express **15**, 924 (2007).
[26] T. A. Ibrahim, K. Amarnath, L. C. Kuo, R. Grover, V. Van, and P. T. Ho, Opt. Lett. **29**, 2779 (2004).
[27] N. Sherwood-Droz, H. Wang, L. Chen, B. G. Lee, A. Biberman, K. Bergman, and M. Lipson, Opt. Express **16**, 15915 (2008).
[28] J. Topolancik and F. Vollmer, Appl. Phys. Lett. **89**, 184103 (2006).
[29] J. Topolancik and F. Vollmer, Biophys. J. **92**, 2223 (2007).
[30] D. Oesterhelt, C. Bräuchle, and N. Hampp, Q. Rev. Biophys. **24**, 425 (1991).
[31] N. Hampp, Chem. Rev. **100**, 1755 (2000).
[32] S. Roy, C. P. Singh, and K. P. J. Reddy, J. Appl. Phys. **90**, 3679 (2001).
[33] K. J. Wise, N. B. Gillespie, J. A. Stuart, M. P. Krebs, and R. R. Birge, Trends Biotechnol. **20**, 387 (2002).
[34] R. R. Birge, N. B. Gillespie, E. W. Izaguirre, A. Kusnetzow, A. F. Lawrence, D. Singh, Q. W. Song, E. Schmidt, J. A. Stuart, S. Seetharaman, and K. J. Wise, J. Phys. Chem. B **103**, 10746 (1999).
[35] J. A. Stuart, D. L. Mercy, K. J. Wise, and R. R. Birge, Synth. Met. **127**, 3 (2002).
[36] C. P. Singh and S. Roy, Opt. Commun. **218**, 55 (2003).
[37] P. Sharma and S. Roy, J. Appl. Phys. **96**, 1687 (2004).
[38] P. Sharma and S. Roy, IEEE Trans. Nanobiosci. **3**, 129 (2004).
[39] D. K. Gayen and J. N. Roy, Appl. Opt. **47**, 933 (2008).
[40] Z. Y. Shen and L. L. Wu, Appl. Opt. **47**, 3737 (2008).
[41] A. Kodi and A. Louri, Appl. Opt. **48**, E13 (2009).
[42] H. J. Caulfield, R. A. Soref, and C. S. Vikram, Photonics Nanostruct. Fundam. Appl. **5**, 14 (2007).